Electronic Supplementary Material (ESI) for Inorganic Chemistry Frontiers.
This journal is © the Partner Organisations 2021

Supporting Information

A ferroelastic molecular rotor crystal showing inverse temperature symmetry breaking

Le-Ping Miao[a†], Lin-Lin Chu[b†], Xiang-Bin Han[a†], Bei-Dou Liang[a], Chao-Yang Chai[a], Chang-Chun Fan[a], Xiao-Xu Wang*[c], Ye-Feng Yao*[b], Wen Zhang*[a]

[a] Jiangsu Key Laboratory for Science and Applications of Molecular Ferroelectrics and School of Chemistry and Chemical Engineering, Southeast University, Nanjing 211189, China

[b] Department of Physics & Shanghai Key Laboratory of Magnetic Resonance, School of Physics and Materials Science, East China Normal University, Shanghai 200062, China

[c] Beijing Key Laboratory of Cloud Computing Key Technology and Application, Beijing Computing Center, Beijing Academy of Science and Technology, Beijing 100094, China

E-mail: wangxx@bcc.ac.cn; yfyao@phy.ecnu.edu.cn; zhangwen@seu.edu.cn

† The authors contributed equally.

Experimental

Figure S1. TGA curve of **1**.

Figure S2. Views of crystal packings of **1** at 243 K. H atoms are omitted for clarity.

Figure S3. Hirshfeld surfaces of **1** at 123 and 373 K. Red, white and blue regions of the Hirshfeld surfaces indicate positive (close contact), neutral and negative isoenergies, respectively.

Figure S4. Asymmetric unit of the crystal structure of **1** in the LTP (93 K) and HTP (373 K) and the packing in the HTP.

Figure S5. Normal thermal expansion of the *b* and *c* axes.

Figure S6. Atomic displacement ellipsoids of the dabco and peripheral ^{t}Bu groups in **1**.

Figure S7. Differential scanning calorimetry measurement of **1**. Note: the start-up hook at 285 K is not related to the phase transition.

Figure S8. Variable-temperature powder X-ray diffraction patterns measured between 248 K and 290 K. The peaks with * are from sample holder.

Figure S9. Characteristic Pake patterns of the dabco rotator.

Figure S10. Simulated ^{13}C chemical shift anisotropy powder patterns of the $-CH_3$ of ^{t}Bu.

Figure S11. Microscope image of a single crystal of **1** (Scale division = 0.2 mm).

Figure S12. Schematic illustration of one type of twin in the monoclinic phase of **1** with reversal of the crystallographic *c* axis at the wall ($+c \rightarrow -c$).

Figure S13. Top and side views of the molecule structure of crystal **2** at 120 K and 293 K.

Figure S14. Views of crystal packings of **2** at 120 K. The yellow box indicates the layer structure in the *ab* plane. H atoms are omitted for clarity.

Figure S15. Views of molecular packings in one layer of **2** at 120 K in a combined capped sticks and spacefill style. H atoms are omitted for clarity.

Figure S16. Rotational barriers of the axial rotator dabco based on the crystal structures of **2** at 120 and 293 K, respectively. The rotation angel is set in 0−120° range due to the ideal C_3 symmetry of the rotator.

Table S1. Crystallographic data and structural refinement details for **1**−**2**.

Table S2. Selected bond lengths [Å] and angles [°] for **1** (93 K, 263 K, 293 K) and **2** (120 K, 293 K).

Table S3. The ε_{31} component of the strain tensor of **1**.

Experimental

Materials and general characterizations. Reagents used were in analytical grade without further purification. D_2O (99.8 atom % D) was purchased from J&K Scientific. Mass spectrometry test was performed on a high-performance liquid-phase time-of-flight mass spectrometer (1260-6224, Agilent). Powder X-ray diffraction patterns were obtained on a Rigaku SmartLab X-ray diffraction instrument Ultima IV. Differential scanning calorimetry measurement was carried out on a TA Instruments SDT-Q10 at a scanning rate of 10 K min^{-1} under nitrogen. Thermogravimetric analysis (TGA) was performed by a TG209 F3 system (NETZSCH). Specific heat capacity was measured on a Quantum Design PPMS-9 (Quantum Design). Ferroelastic domain measurement of single crystals was carried out by an Olympus BX51TRF optical polarizing microscope, equipped with an INSTEC mK 1000 hot and cold stage.

Synthesis. $[Zn(saloph)]_2$ was synthesized according to a reported procedure.[1] The orange block crystals of **1** were obtained by a slow evaporation of a mixed DMF-EtOH (v:v = 1:1) solution of $[Zn(saloph)]_2$ (1.0 g, 1.7 mmol) and dabco (0.09 g, 0.83 mmol), with a yield of 60% (based on dabco). Compound **2** was prepared with the similar method with a yield of 55%. The deuterated dabco (MS: d8-dabco, 100%) was synthesized according to a reported method,[2] which was used in the sysnthesis of the dabco-deuterated crystalline sample for ^2H NMR experiments.

Single-crystal X-ray Diffraction. Crystallographic data of the salts were collected at on a Rigaku Oxford Diffraction Supernova Dual Source, Cu at Zero equipped with an AtlasS2 CCD using Cu and Mo Kα radiation and XtaLAB Synergy R, DW system equipped with an HyPix CCD using Mo Kα radiation. The Rigaku CrysAlisPro was used to collect Data, refine cell, and to reduce data. SHELXL-2014 software package was used to solve the structures by direct methods. All non-hydrogen atoms were refined anisotropically. The details of crystal data are given in Tables S1 and S2. It is notable that pseudosymmetry is detected in the structures solved at 263, 273, 283, and 293 K in which a *C*2/*c* space

group is suggested. This elert may originate from the disorder of the ^{t}Bu groups in the HTP.

CCDC 2032939−2032945, 2032947−2032953 and 2033283−2033284 contain the crystallographic data for **1** and **2**. These data can be obtained free of charge via http://www.ccdc.cam.ac.uk/conts/retrieving.html, or from the Cambridge Crystallographic Data Centre, 12 Union Road, Cambridge CB2 1EZ, UK; fax: +44 1223-336-033; or e-mail: deposit@ccdc.cam.ac.uk.

Solid-state NMR measurements. Variable-temperature solid state ^{1}H-^{13}C CP/MAS NMR experiments were performed on a Bruker AVANCE III 400 WB spectrometer operating at 400.13 MHz and 100.62 MHz for ^{1}H and ^{13}C, respectively. A 4 mm double resonance MAS probe was used for the ^{13}C experiments. The ^{1}H 90^o pulse was 2.5 μs and the ^{13}C 90^o pulse was 4.0 μs. The ^{1}H two-pulse phase modulation (TPPM) decoupling was applied during the ^{13}C signal acquisition. To facilitate the temperature regulation, the spin rate of rotor was set to 2.5 kHz. In order to suppress the spinning sidebands, the pulse sequence "cptoss" was used in the experiments. The ^{13}C chemical shift anisotropy (CSA) patterns were recorded by using the pulse sequence "SUPER" (separation of undistorted powder patterns by effortless recoupling[3]). The spin rate in the SUPER experiments was set to 2.5 kHz too. The ^{13}C chemical shifts were calibrated using adamantane (δ = 38.5 ppm).

Variable-temperature ^{2}H NMR experiments were carried out on a Bruker AVANCE III 300 WB spectrometer operating at 46.01 MHz for ^{2}H. A static probe was used in the experiments. The solid-echo pulse sequence was used to record the spectra. The ^{2}H 90° pulse was 2.5 μs. The echo delays in the experiments were varied between 20 μs and 25 μs. The recycle delay was set to 0.4 s. The ^{2}H NMR pattern simulation was obtained by using NMR Weblab (https://weblab2.mpip-mainz.mpg.de/weblab66/weblab.html).

Computing method. By the *Vienna Ab initio* Simulation Package (VASP)[4,5] of density functional theory (DFT), the rotational barriers of axial and peripheral rotators are calculated based on crystal structures at

93, 293 and 373 K, respectively, via a rigid scan mode. The projector augmented wave (PAW) method,[6] and the generalized gradient approximation (GGA) in the Perdew–Burke–Ernzerhof (PBE) form[7,8] were carried out. A cutoff energy of 600 eV was adopted for all simulations. During structure relaxation, the energy converged to 1.0×10^5 eV/atom, and the force convergence condition was 0.01eV/Å. The Brillouin zone was sampled using a Monkhorst–Pack k-point mesh of 1×2×1 for structure relaxation and energy calculations, respectively.

References

1. Kleij, A. W.; Kuil, M.; Tooke, D. M.; Lutz, M.; Spek, A. L.; Reek, J. N. H. Zn^{II}–Salphen Complexes as Versatile Building Blocks for the Construction of Supramolecular Box Assemblies. *Chem. Eur. J.* **2005**, *11*, 4743−4750.
2. Catalano, L.; Pérez-Estrada, S.; Terraneo, G.; Pilati, T.; Resnati, G.; Metrangolo, P.; Garcia-Garibay, M. A. Dynamic Characterization of Crystalline Supramolecular Rotors Assembled through Halogen Bonding. *J. Am. Chem. Soc.* **2015**, *137*, 15386−15389.

3 Liu, S.-F.; Mao, J.-D.; Schmidt-Rohr, K. A Robust Technique for Two-Dimensional Separation of Undistorted Chemical-Shift Anisotropy Powder Patterns in Magic-Angle-Spinning NMR. *J. Magn. Reson.* **2002**, *155*, 15−28.

4 Kresse, G.; Furthmüller, J. Efficient iterative schemes for ab initio totalenergy calculations using a plane-wave basis set. *Phys. Rev. B* **1996**, *54*, 11169−11186.

5 Kresse, G.; Joubert, D. From ultrasoft pseudopotentials to the projector augmented-wave method. *Phys. Rev. B* **1999**, *59*, 1758−1775.

6 Blöchl, P. E. Projector augmented-wave method. *Phys. Rev. B* **1994**, *50*, 17953−17979.

7 Perdew, J. P.; Chevary, J. A.; Vosko, S. H.; Jackson, K. A.; Pederson, M. R.; Singh, D. J.; Fiolhais, C. Atoms, Molecules, Solids, and Surfaces: Applications of the Generalized Gradient Approximation for Exchange and Correlation. *Phys. Rev. B* **1992**, *46*, 6671−6687.

8 Perdew, J. P.; Wang, Y. Accurate and simple analytic representation of the electron-gas correlation energy. *Phys. Rev. B* **1992**, *45*, 13244−13249.

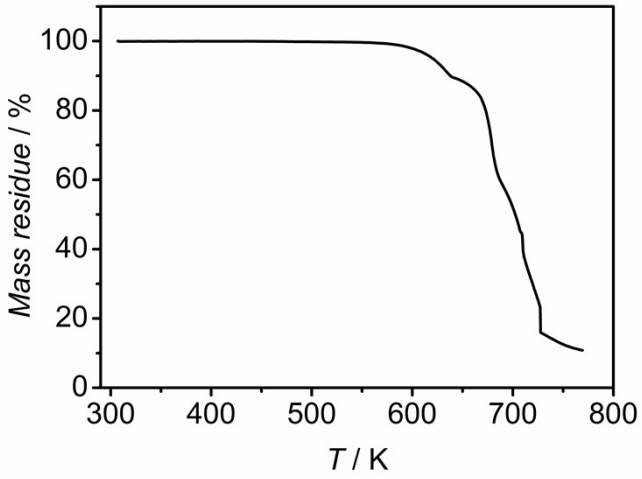

Figure S1. TGA curve of **1**.

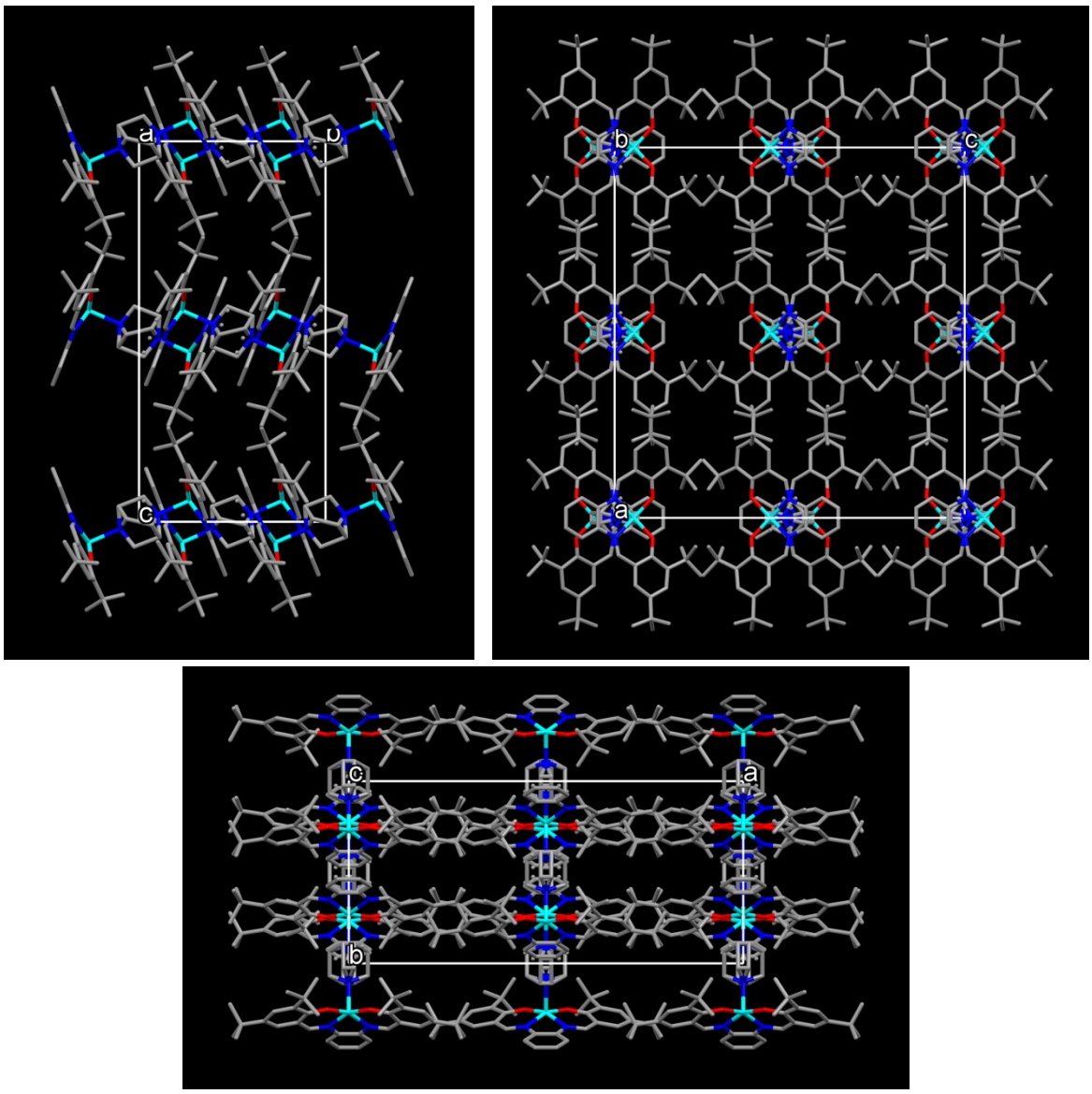

Figure S2. Views of crystal packings of **1** at 243 K. H atoms are omitted for clarity.

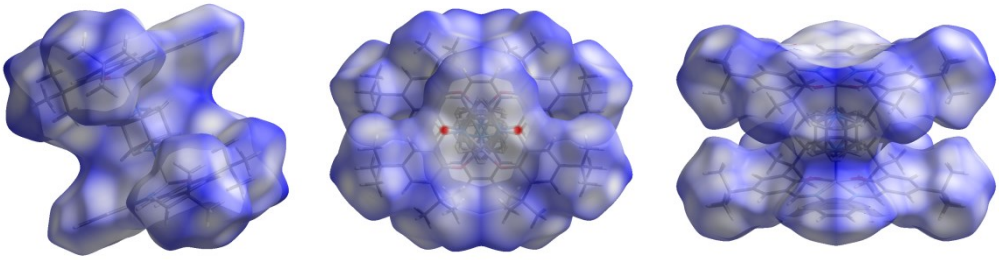

123 K

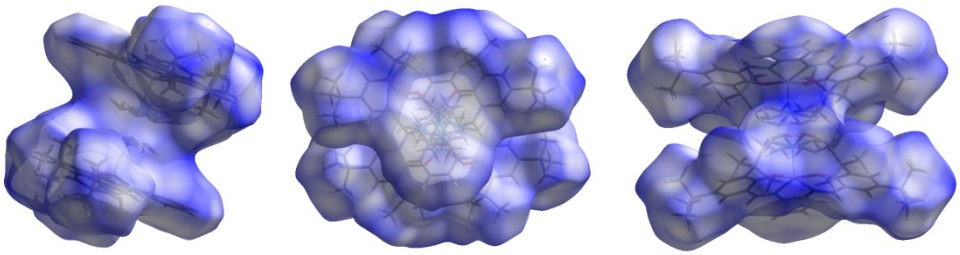

373 K

Figure S3. Hirshfeld surfaces of **1** at 123 and 373 K. Red, white and blue regions of the Hirshfeld surfaces indicate positive (close contact), neutral and negative isoenergies, respectively.

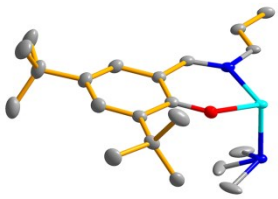

LTP

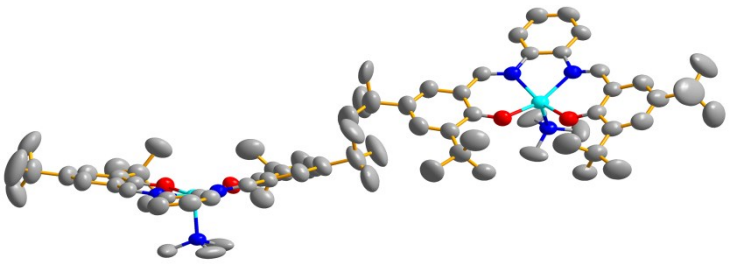

HTP

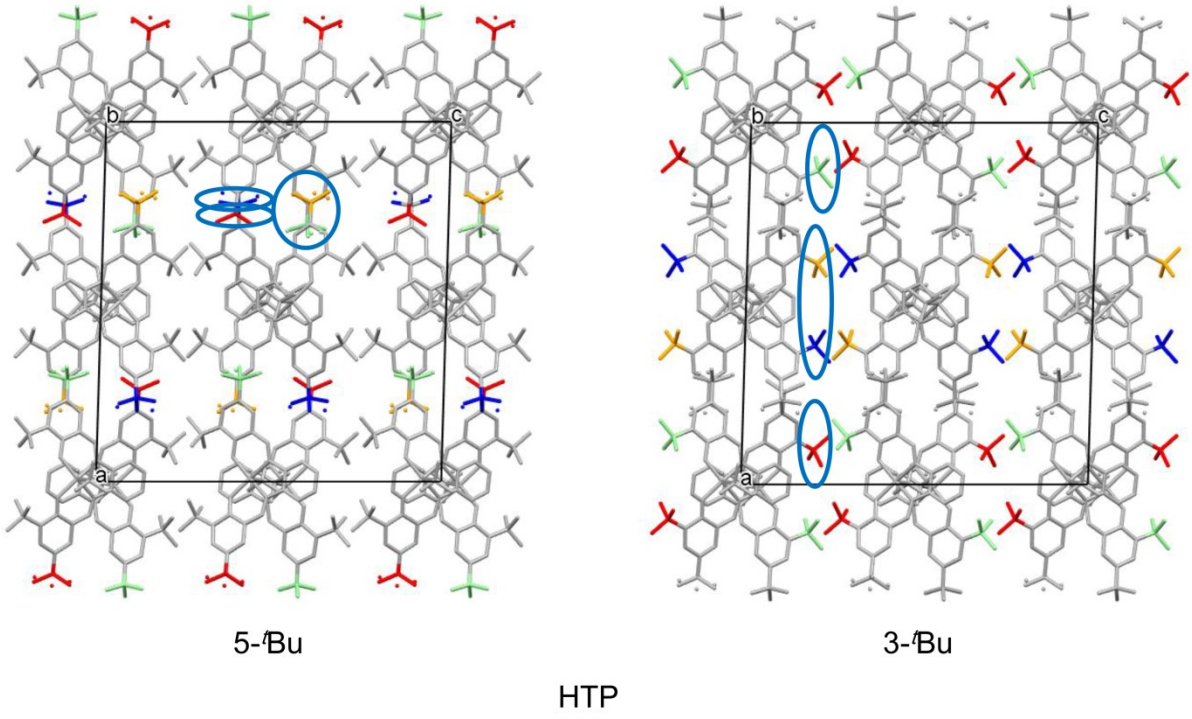

Figure S4. Asymmetric unit of the crystal structure of **1** in the LTP (93 K) and HTP (373 K) and the packing in the HTP.

Note: The asymmetric *tert*-butyl groups in the HTP are differently colored. Due to ITSB, the local environments around the *tert*-butyl groups become different. Thus, the *tert*-butyl groups can be roughly classified into three types with ratio of 1:1:2, as indicated by the dark blue circles.

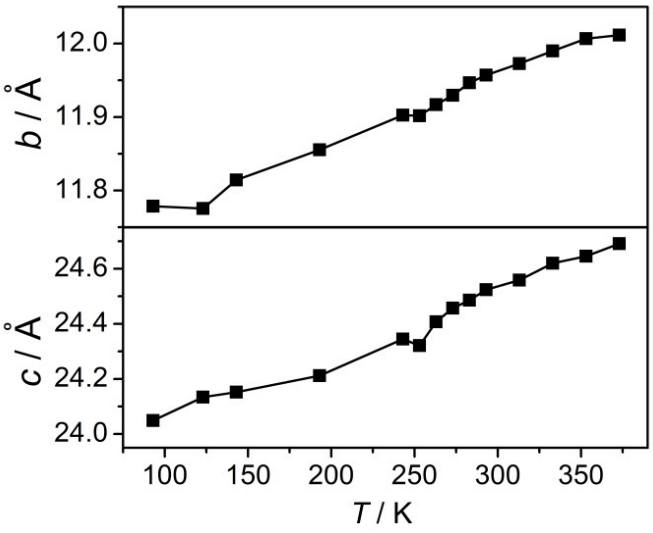

Figure S5. Normal thermal expansion of the *b* and *c* axes.

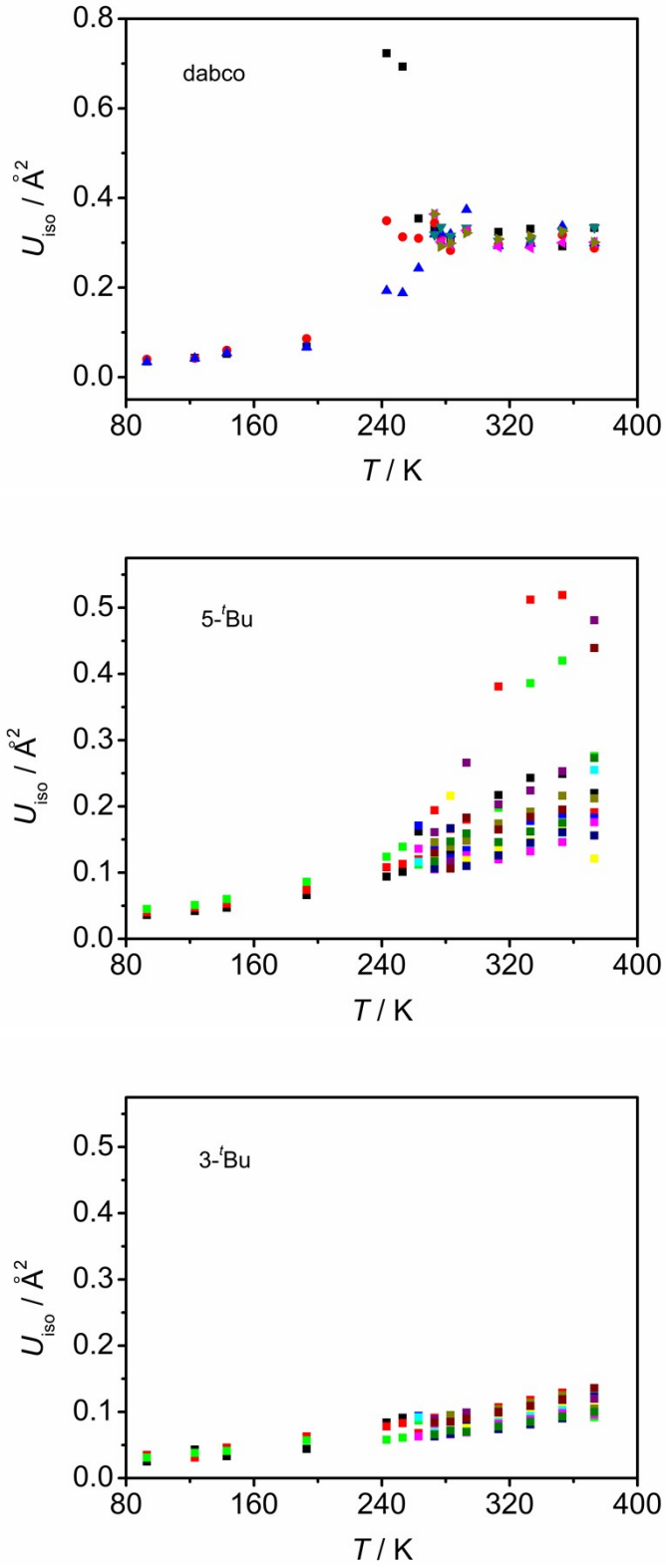

Figure S6. Atomic displacement ellipsoids of the dabco and peripheral ^{t}Bu groups in **1**.

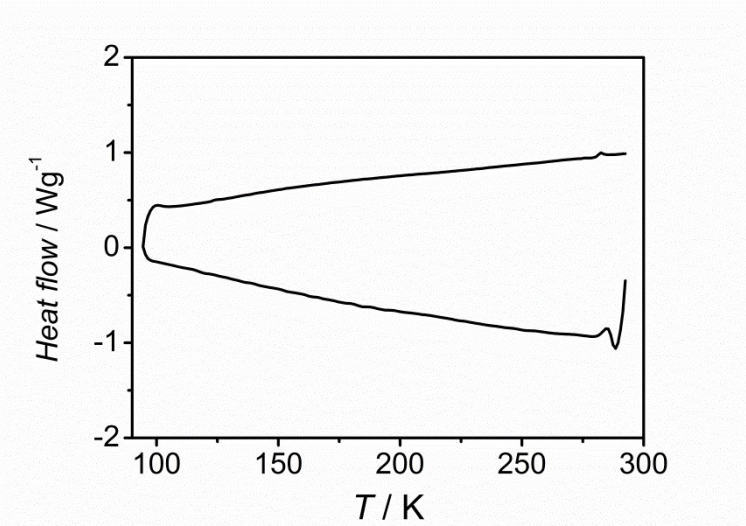

Figure S7. Differential scanning calorimetry measurement of **1**. Note: the start-up hook at 285 K is not related to the phase transition.

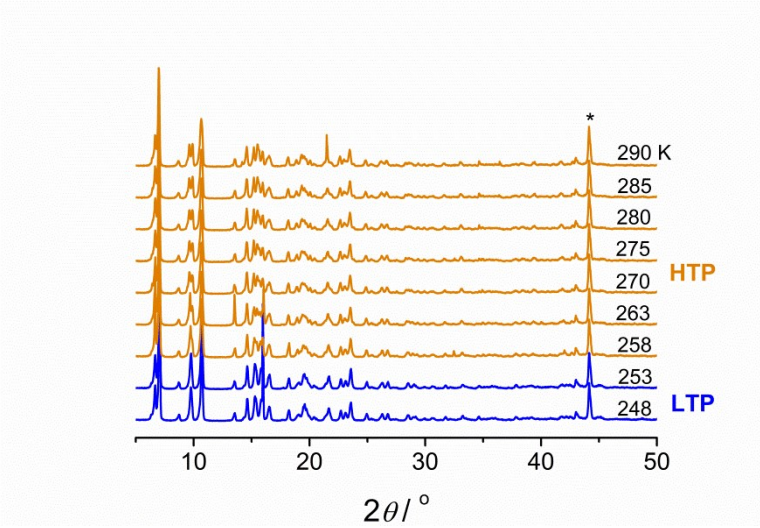

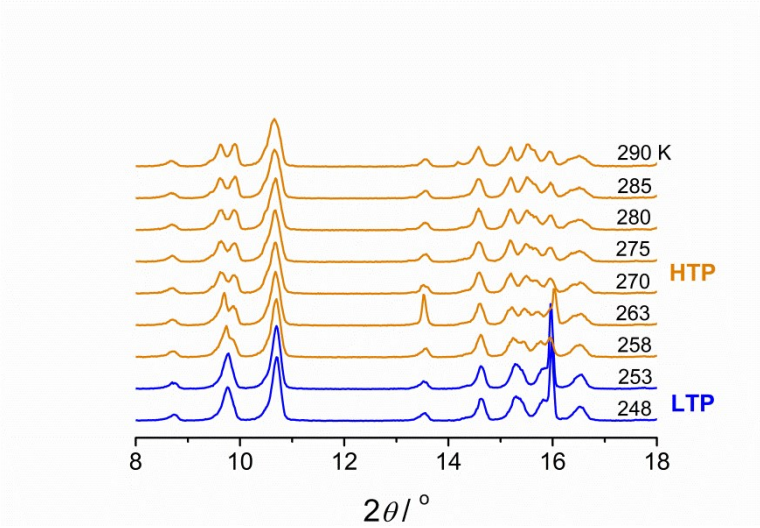

Figure S8. Variable-temperature powder X-ray diffraction patterns measured between 248 K and 290 K. The peaks with * are from sample holder.

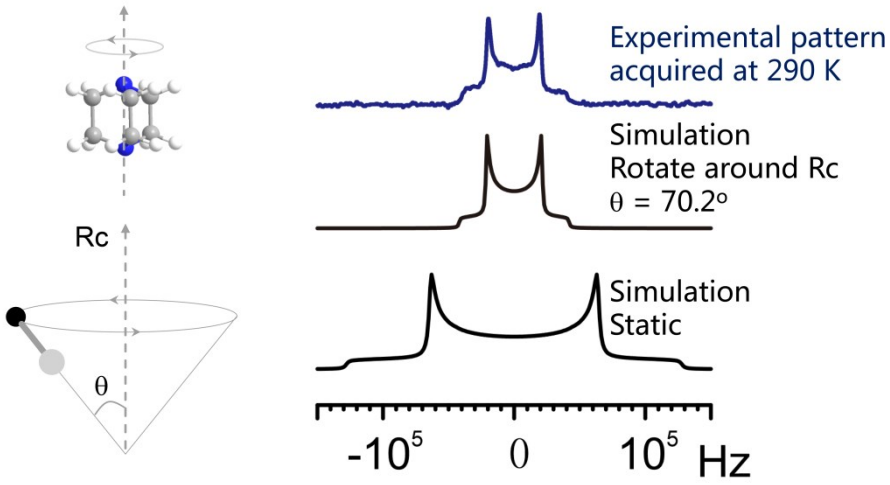

Figure S9. Characteristic Pake patterns of the dabco rotator.

Left: the cartoon picture of the rotation of dabco. Right: The deep blue line: the experimental ^{2}H pattern acquired at 290 K. The black lines: the simulated ^{2}H patterns using the model described by the cartoon picture in the left. The patterns show the typical Pake lineshape. The wide one was simulated assuming that the dabco molecule is static and the narrow one was simulated assuming that the dabco molecule undergos a local axial rotation around Rc with an incline angle θ of 70.2°.

The two simulated patterns clearly demonstrate the motional effects on the ^{2}H patterns. The very similar lineshahpe between the experimental pattern and the simulated one by using the axial rotational model indicates that the dabco molecule most likely underdoes the axial rotation at 290 K.

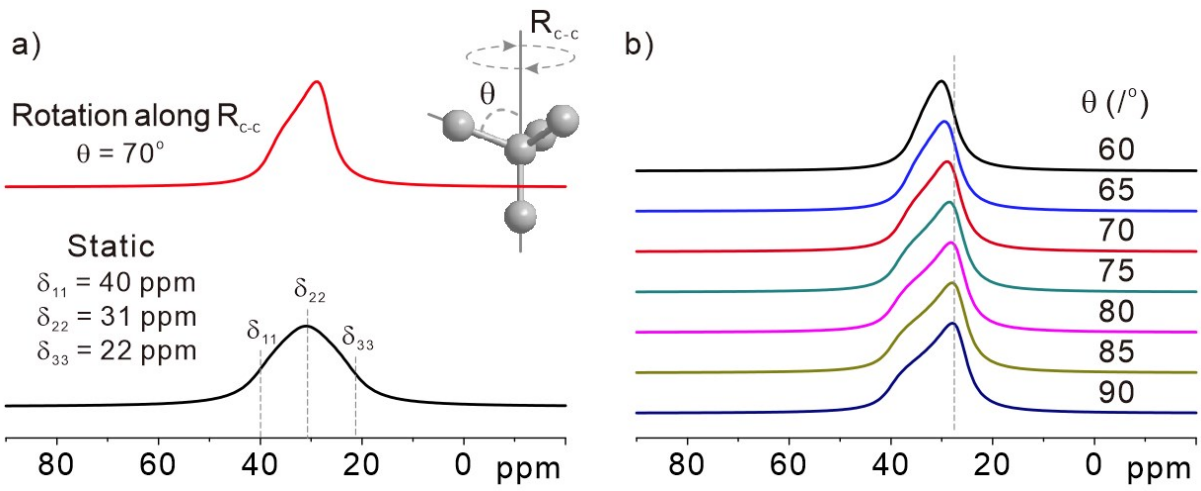

Figure S10. Simulated ^{13}C chemical shift anisotropy powder patterns of the $-CH_3$ of ^{t}Bu. a) The black one is simulated under the condition that the ^{t}Bu group does not rotate along the Rc-c axis, while the red one is simulated under the condition that the ^{t}Bu group rotates along the R_{c-c} axis. b) The dependence of the angle θ (see the cartoon picture). The ^{13}C chemical shift anisotropy parameters (δ_{11} = 40 ppm, δ_{22} = 31 ppm, δ_{33} = 22 ppm) used in the simulations are determined from the experiment (see Figure 3).

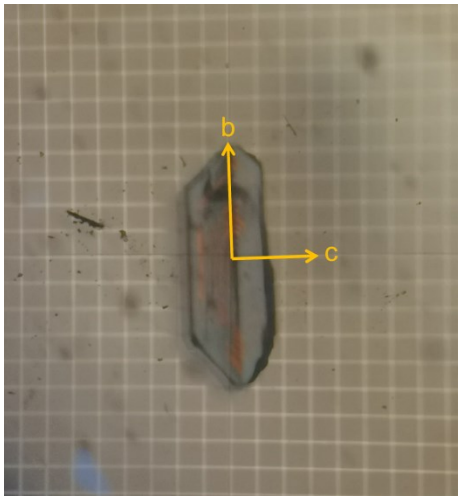

Figure S11. Microscope image of a single crystal of **1** (Scale division = 0.2 mm).

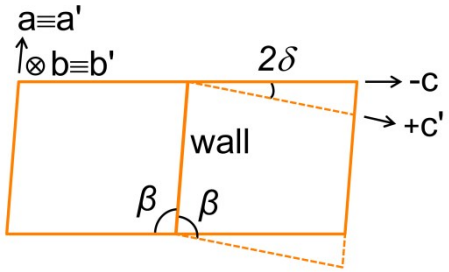

Figure S12. Schematic illustration of one type of twin in the monoclinic phase of **1** with reversal of the crystallographic *c* axis at the wall (+*c*→−*c*).

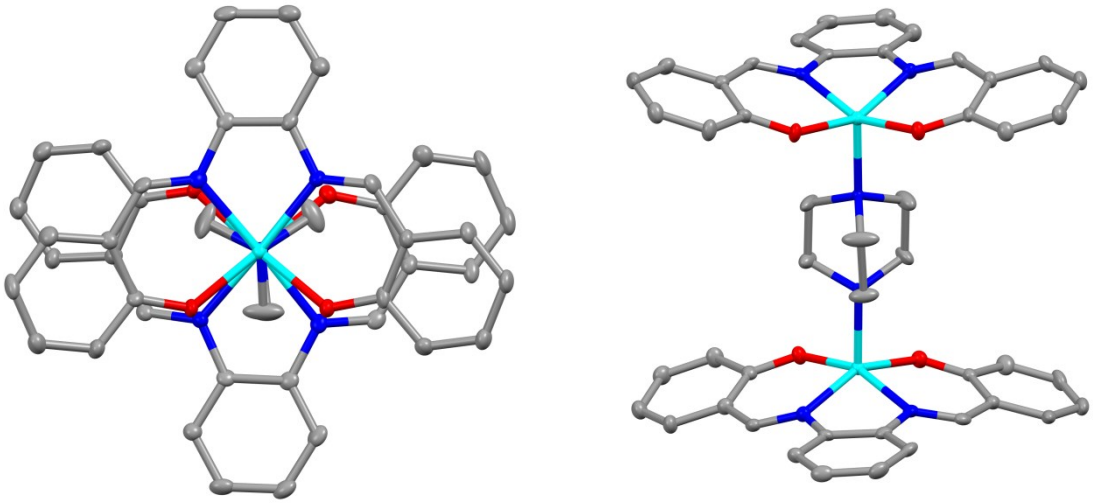

120 K

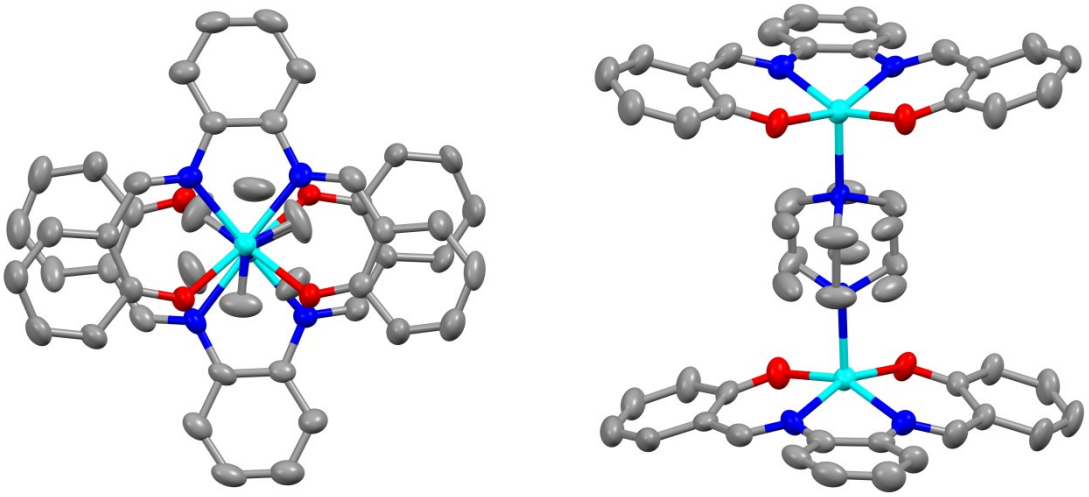

293 K

Figure S13. Top and side views of the molecule structure of crystal **2** at 120 K and 293 K.

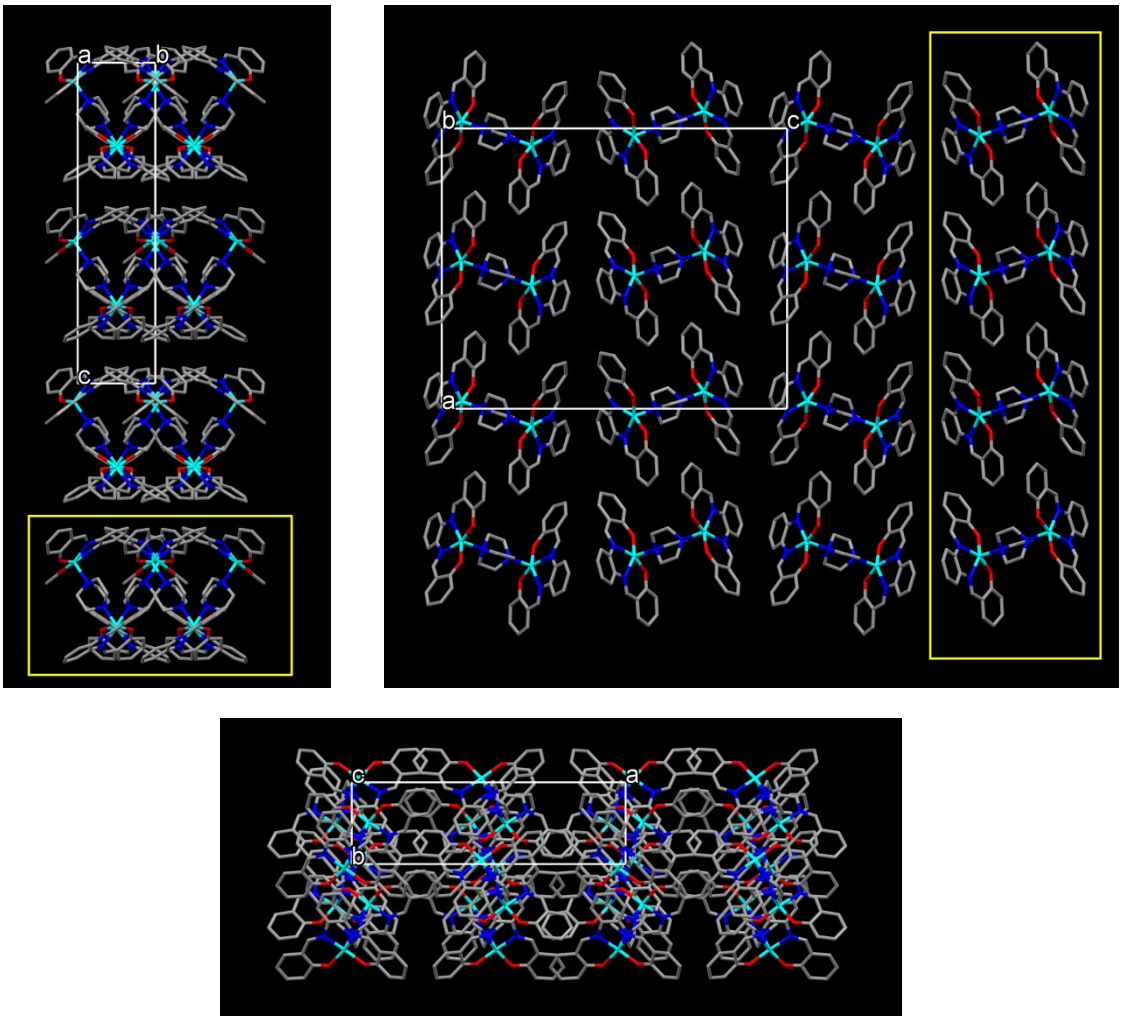

Figure S14. Views of crystal packings of **2** at 120 K. The yellow box indicates the layer structure in the *ab* plane. H atoms are omitted for clarity.

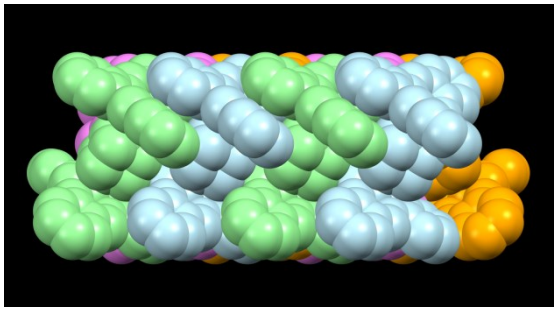

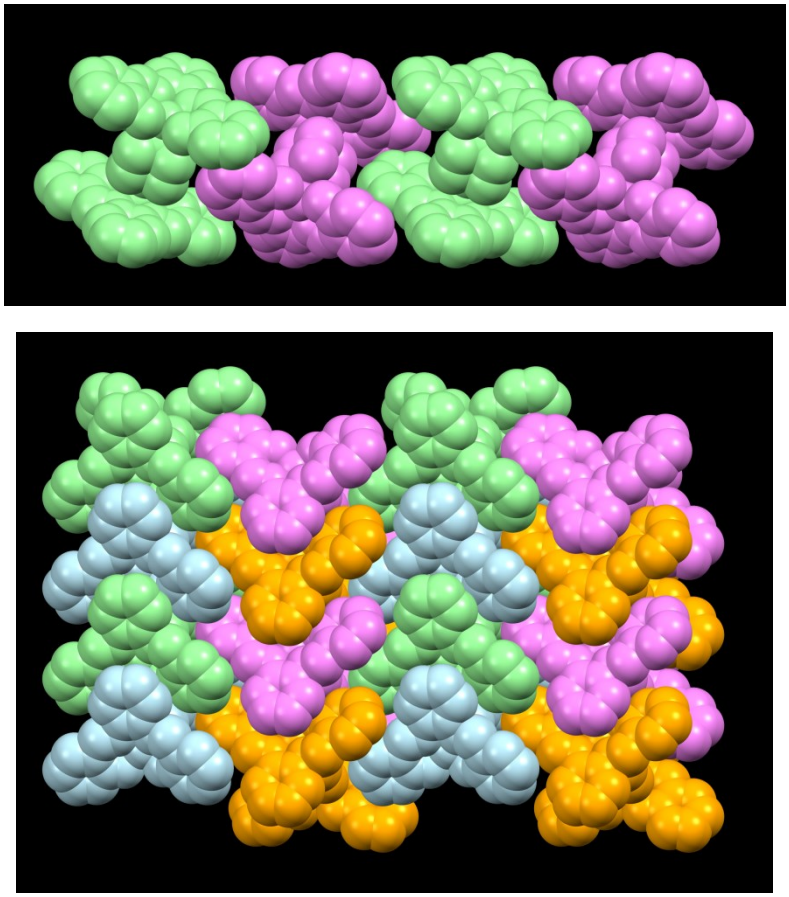

Figure S15. Views of molecular packings in one layer of **2** at 120 K in a combined capped sticks and spacefill style. H atoms are omitted for clarity.

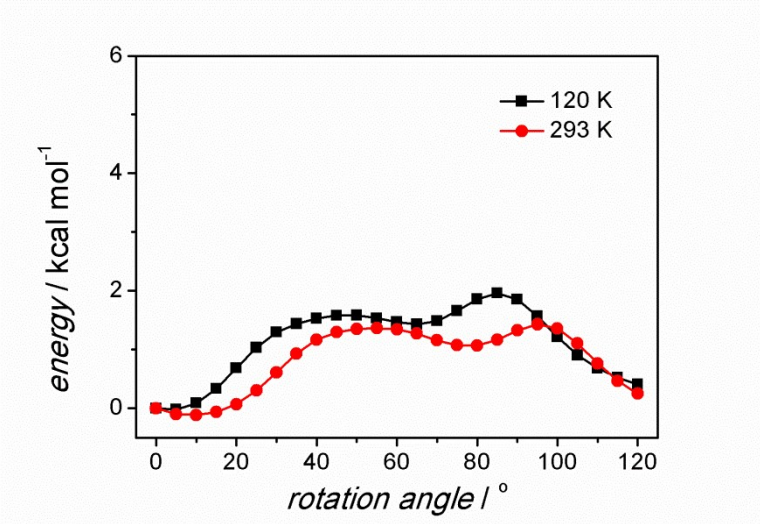

Figure S16. Rotational barriers of the axial rotator dabco based on the crystal structures of **2** at 120 and 293 K, respectively. The rotation angel is set in 0−120° range due to the ideal C_3 symmetry of the rotator.

Table S1. Crystallographic data and refinement parameters for **1** and **2**.

1	**93 K**	**123 K**	**143 K**	**193 K**
formula	$C_{78}H_{104}N_6O_4Zn_2$	$C_{78}H_{104}N_6O_4Zn_2$	$C_{78}H_{104}N_6O_4Zn_2$	$C_{78}H_{104}N_6O_4Zn_2$
M_w	1320.46	1320.46	1320.46	1320.46
Crystal system	Orthorhombic	Orthorhombic	Orthorhombic	Orthorhombic
space group	*Cmca*	*Cmca*	*Cmca*	*Cmca*
a [Å]	25.7813(7)	25.7774(10)	25.7941(5)	25.7627(7)
b [Å]	11.7785(3)	11.7754(4)	11.8142(2)	11.8554(3)
c [Å]	24.0488(5)	24.1337(8)	24.1521(5)	24.2120(7)
α [º]	90	90	90	90
β [º]	90	90	90	90
γ [º]	90	90	90	90
V [Å^3]	7302.8(3)	7325.5(4)	7360.0(2)	7395.0(3)
Z	4	4	4	4
ρ_{calcd} [g cm^{-3}]	1.201	1.197	1.192	1.186
μ [mm^{-1}]	0.708	0.706	0.703	0.699
total reflns	20934	15155	21175	21204
obsd reflns ($I > 2\sigma(I)$)	5759	5415	5850	5728
R_{int}	0.0185	0.0540	0.0220	0.0203
R_1[a], wR_2[b] ($I > 2\sigma(I)$)	0.0285, 0.0715	0.0461, 0.1131	0.0296, 0.0737	0.0346, 0.0904
R_1[a], wR_2[b] (all data)	0.0326, 0.073	0.0694, 0.1219	0.0339, 0.0755	0.0409, 0.0932
GOF (F^2)	1.085	1.078	1.060	1.095
$\Delta\rho$[c] [e Å^{-3}]	0.374/−0.401	0.671/−1.307	0.360/−0.401	0.458/−0.588

1	**243 K**	**253 K**	**263 K**	**273 K**
formula	$C_{78}H_{104}N_6O_4Zn_2$	$C_{78}H_{104}N_6O_4Zn_2$	$C_{78}H_{104}N_6O_4Zn_2$	$C_{78}H_{104}N_6O_4Zn_2$
M_w	1320.46	1320.46	1320.46	1320.46
Crystal system	Orthorhombic	Orthorhombic	Monoclinic	Monoclinic
space group	*Cmca*	*Cmca*	$P2_1/c$	$P2_1/c$
a [Å]	25.7519(9)	25.7429(11)	25.7309(10)	25.6667(8)
b [Å]	11.9026(3)	11.9016(4)	11.9168(4)	11.9295(3)
c [Å]	24.3448(6)	24.3208(8)	24.4073(7)	24.4570(6)
α [º]	90	90	90	90
β [º]	90	90	91.045(3)	91.295(2)
γ [º]	90	90	90	90
V [Å^3]	7462.0(4)	7451.4(5)	7482.8(4)	7486.6(4)
Z	4	4	4	4
ρ_{calcd} [g cm^{-3}]	1.165	1.166	1.172	1.171
μ [mm^{-1}]	0.693	0.694	0.691	0.691
total reflns	19347	23227	65892	70843
obsd reflns ($I > 2\sigma(I)$)	5814	5819	23057	23011
R_{int}	0.0202	0.0310	0.0361	0.0313
R_1[a], wR_2[b] ($I > 2\sigma(I)$)	0.0402, 0.1109	0.0445, 0.1173	0.0529, 0.1307	0.0482, 0.1104

R_1[a], wR_2[b] (all data)	0.0518, 0.1163	0.0593, 0.1242	0.1044, 0.1528	0.0888, 0.1268
GOF (F^2)	1.078	1.057	1.005	1.014
$\Delta\rho$[c] [e Å^{-3}]	0.516/−0.570	0.432/−0.496	0.374/−0.569	0.298/−0.608

1	**283 K**	**293 K**	**313 K**
formula	$C_{78}H_{104}N_6O_4Zn_2$	$C_{78}H_{104}N_6O_4Zn_2$	$C_{78}H_{104}N_6O_4Zn_2$
M_w	1320.46	1320.46	1320.46
Crystal system	Monoclinic	Monoclinic	Monoclinic
space group	$P2_1/c$	$P2_1/c$	$P2_1/c$
a [Å]	25.6658(7)	25.6779(6)	25.6749(7)
b [Å]	11.9465(3)	11.9570(2)	11.9727(2)
c [Å]	24.4857(7)	24.5237(5)	24.5587(6)
α [°]	90	90	90
β [°]	91.355(2)	91.496(2)	91.535(2)
γ [°]	90	90	90
V [Å^3]	7505.6(4)	7527.0(3)	7546.6(3)
Z	4	4	4
ρ_{calcd} [g cm^{-3}]	1.169	1.165	1.162
μ [mm^{-1}]	0.689	0.687	0.685
total reflns	75181	79341	74199
obsd reflns ($I > 2\sigma(I)$)	23100	23448	23492
R_{int}	0.0348	0.0334	0.0347
R_1[a], wR_2[b] ($I > 2\sigma(I)$)	0.0510, 0.1137	0.0505, 0.1124	0.0515, 0.1169
R_1[a], wR_2[b] (all data)	0.0887, 0.1285	0.0873, 0.1267	0.0916, 0.1335
GOF (F^2)	1.024	1.021	1.006
$\Delta\rho$[c] [e Å^{-3}]	0.295/−0.612	0.264/−0.596	0.297/−0.603

1	**333 K**	**353 K**	**373 K**
formula	$C_{78}H_{104}N_6O_4Zn_2$	$C_{78}H_{104}N_6O_4Zn_2$	$C_{78}H_{104}N_6O_4Zn_2$
M_w	1320.46	1320.46	1320.46
Crystal system	Monoclinic	Monoclinic	Monoclinic
space group	$P2_1/c$	$P2_1/c$	$P2_1/c$
a [Å]	25.6792(8)	25.7068(9)	25.6537(9)
b [Å]	11.9900(3)	12.0066(4)	12.0116(3)
c [Å]	24.6202(6)	24.6453(9)	24.6910(8)
α [°]	90	90	90
β [°]	91.580(2)	91.649(3)	91.542 (3)
γ [°]	90	90	90
V [Å^3]	7577.5(4)	7603.7(5)	7605.6(4)
Z	4	4	4
ρ_{calcd} [g cm^{-3}]	1.158	1.153	1.153
μ [mm^{-1}]	0.683	0.680	0.680
total reflns	78694	75172	77537

obsd reflns ($I > 2\sigma(I)$)	23593	23661	23581
R_{int}	0.0351	0.0403	0.0463
R_1[a], wR_2[b] ($I > 2\sigma(I)$)	0.0542, 0.1164	0.0587, 0.1273	0.0604, 0.1266
R_1[a], wR_2[b] (all data)	0.0974, 0.1337	0.1108, 0.1470	0.1170, 0.1477
GOF (F^2)	1.035	1.040	1.029
$\Delta\rho$[c] [e Å^{-3}]	0.283/−0.464	0.268/−0.497	0.293/−0.508

2	**120K**	**293K**
formula	C_{46} H_{40} N_6 O_4 Zn_2	C_{46} H_{40} N_6 O_4 Zn_2
M_w	871.62	871.62
Crystal system	Orthorhombic	Orthorhombic
space group	$Pca2_1$	$Pca2_1$
a [Å]	21.8463(4)	21.837(2)
b [Å]	6.49341(12)	6.5767(6)
c [Å]	27.0149(5)	27.229(2)
α [°]	90	90
β [°]	90	90
γ [°]	90	90
V [Å^3]	3832.25(12)	3910.5(6)
Z	4	4
ρ_{calcd} [g cm^{-3}]	1.511	1.480
μ [mm^{-1}]	1.983	1.281
total reflns	26729	17939
obsd reflns ($I > 2\sigma(I)$)	7716	10999
R_{int}	0.0831	0.0700
R_1[a], wR_2[b] ($I > 2\sigma(I)$)	0.0473, 0.1143	0.0634, 0.1107
R_1[a], wR_2[b] (all data)	0.0549, 0.1215	0.1069, 0.1319
GOF (F^2)	1.019	0.970
$\Delta\rho$[c] [e Å^{-3}]	0.572/−0.650	0.443/−0.944

[a] $R_1 = \Sigma| |F_o| - |F_c| | / |F_o|$. [b] $wR_2 = [\Sigma w(F_o^2 - F_c^2)^2] / \Sigma w(F_o^2)^2]^{1/2}$. [c] Maximum and minimum residual electron density.

Table S2. Selected bond lengths [Å] and angles [°] for **1** (93 K, 293 K) and **2** (120 K, 293 K).

1 (93 K)			
N2−Zn1	2.1686(13)	O1−Zn1−O1^i	92.72(5)
O1−Zn1	1.9474(8)	O1−Zn1−N1^i	158.84(4)
Zn1−O1^i	1.9474(8)	O1^i−Zn1−N1^i	90.29(4)
		O1−Zn1−N1	90.29(4)
		O1^i−Zn1−N1	158.84(4)
		N1^i−Zn1−N1	79.70(5)
		O1−Zn1−N2	100.47(3)
		O1^i−Zn1−N2	100.47(3)
		N1^i−Zn1−N2	99.56(4)

		N1−Zn1−N2	99.56(4)

Symmetry code: (i) −x+2, y, z

1 (293 K)

N1−Zn1	2.0709(17)	O2−Zn1−O1	93.80(6)
N2−Zn1	2.0781(16)	O2−Zn1−N1	156.05(6)
N3−Zn2	2.0760(17)	O1−Zn1−N1	90.01(6)
N4−Zn2	2.0735(16)	O2−Zn1−N2	89.85(6)
N5−Zn1	2.1798(15)	O1−Zn1−N2	160.23(6)
N6−Zn2	2.1804(15)	N1−Zn1−N2	79.13(6)
O1−Zn1	1.9490(14)	O2−Zn1−N5	101.36(6)
O2−Zn1	1.9460(15)	O1−Zn1−N5	100.06(6)
O3−Zn2	1.9518(15)	N1−Zn1−N5	101.23(6)
O4−Zn2	1.9476 (14)	N2−Zn1−N5	98.24(6)
		O4−Zn2−O3	93.77(6)
		O4−Zn2−N4	90.31(6)
		O3−Zn2−N4	156.30(6)
		O4−Zn2−N3	160.04(6)
		O3−Zn2−N3	89.74(6)
		N4−Zn2−N3	78.97(6)
		O4−Zn2−N6	99.49(6)
		O3−Zn2−N6	101.84(6)
		N4−Zn2−N6	100.48(6)
		N3−Zn2−N6	99.00(6)
		O2−Zn1−O1	93.80(6)

2 (120 K)

N1−Zn2	2.143(5)	O4−Zn1−O3	95.95(18)
N2−Zn2	2.115(5)	O4−Zn1−N3	153.9(2)
N3−Zn1	2.105(5)	O3−Zn1−N3	89.6(2)
N4−Zn1	2.132(5)	O4−Zn1−N4	89.2(2)
N5−Zn2	2.123(5)	O3−Zn1−N4	158.6(2)
N6−Zn1	2.138(5)	N3−Zn1−N4	77.2(2)
O1−Zn2	1.989(4)	O4−Zn1−N6	100.0(2)
O2−Zn2	1.985(4)	O3−Zn1−N6	99.7(2)
O3−Zn1	1.979(4)	N3−Zn1−N6	104.3(2)
O4−Zn1	1.977(4)	N4−Zn1−N6	99.80(19)
		O2−Zn2−O1	99.39(18)
		O2−Zn2−N2	89.7(2)
		O1−Zn2−N2	156.3(2)
		O2−Zn2−N5	98.2(2)
		O1−Zn2−N5	97.7(2)
		N2−Zn2−N5	102.6(2)
		O2−Zn2−N1	158.6(2)
		O1−Zn2−N1	87.8(2)

		N2−Zn2−N1	76.6(2)
		N5−Zn2−N1	100.72(19)
2 (293 K)			
N1−Zn2	2.100(7)	O4−Zn1−O3	98.3(2)
N2−Zn2	2.119(7)	O4−Zn1−N3	89.6(2)
N3−Zn1	2.100(7)	O3−Zn1−N3	155.1(3)
N4−Zn1	2.129(7)	O4−Zn1−N4	157.9(2)
N5−Zn1	2.145(6)	O3−Zn1−N4	87.9(3)
N6−Zn2	2.132(6)	N3−Zn1−N4	76.7(3)
N5'−Zn1	2.145(6)	O4−Zn1−N5	98.8(2)
N6'−Zn2	2.132(6)	O3−Zn1−N5	99.1(2)
O1−Zn2	1.973(5)	N3−Zn1−N5	102.9(2)
O2−Zn2	1.976(5)	N4−Zn1−N5	101.0(2)
O3−Zn1	1.978(5)	O4−Zn1−N5'	98.8(2)
O4−Zn1	1.975(5)	O3−Zn1−N5'	99.1(2)
N1−Zn2	2.100(7)	N3−Zn1−N5'	102.9(2)
		N4−Zn1−N5'	101.0(2)
		O1−Zn2−O2	97.2(2)
		O1−Zn2−N1	89.4(3)
		O2−Zn2−N1	154.1(3)
		O1−Zn2−N2	158.6(3)
		O2−Zn2−N2	89.2(3)
		N1−Zn2−N2	76.6(3)
		O1−Zn2−N6'	99.4(2)
		O2−Zn2−N6'	99.5(2)
		N1−Zn2−N6'	104.1(2)
		N2−Zn2−N6'	99.6(2)
		O1−Zn2−N6	99.4(2)
		O2−Zn2−N6	99.5(2)
		N1−Zn2−N6	104.1(2)
		N−Zn2−N6	99.6(2)

Table S3. The ε_{31} component of the strain tensor of **1**.

T / K	β / °	ε_{31} (= (β−π/2)/2)	ε_s
93	90	0	0
123	90	0	0
143	90	0	0
193	90	0	0
243	90	0	0
253	90	0	0
263	91.045	0.00912	0.01289

273	91.295	0.0113	0.01598
283	91.355	0.01182	0.01672
293	91.496	0.01306	0.01846
313	91.535	0.0134	0.01894
333	91.58	0.01379	0.0195
353	91.649	0.01439	0.02035
373	91.542	0.01346	0.01903